Comparative SAXS Study of Heated and Alkali-Treated Sisal Fibers

Md. N. Khan,[1] D. K. Bisoyi,[2] J. Shukla[3]

[1]*Department of Physics, Indira Gandhi Institute of Technology, Sarang-759146, Orissa, India*
[2]*Department of Physics, National Institute of Technology, Rourkela-769008, Orissa, India*
[3]*Department of Physics, Government College (Autonomous), Angul-759143, Orissa, India*

Received 18 June 2011; accepted 8 November 2011
DOI 10.1002/app.36460
Published online 22 January 2012 in Wiley Online Library (wileyonlinelibrary.com).

ABSTRACT: The present investigation deals with the fine structural characteristics of heated and alkali-treated sisal fiber using small-angle X-ray scattering (SAXS) technique for nonideal two-phase systems. The SAXS intensities of heated and alkali-treated sisal fibers deviate from Porod's law, indicating that the samples belong to nonideal two-phase systems characterized by continuous variation of electron density at the phase boundary. The macromolecular parameters such as the average periodicity transverse to layers, specific inner surface, volume fractions of void and matter phases, and so on of the samples were evaluated by using one- and three-dimensional correlation functions, which reveal all the information concealed in the slit smeared SAXS patterns. As all the samples under our purview of study have two-phase structure with diffuse phase boundaries, the average thickness of the transition region have been determined. This analysis throws some light on the structural changes that occurred in the dewaxed sisal fiber treated by NaOH solutions and subject to heat treatments. © 2012 Wiley Periodicals, Inc. J Appl Polym Sci 125: 2356–2362, 2012

Key words: correlation functions; SAXS; sisal fiber; transverse periodicity; lamellar model

INTRODUCTION

Small-angle X-ray scattering (SAXS) takes place in a system having particle inhomogeneities of colloidal dimensions. Such large spacings are found in some complex molecules such as cellulose, collagens, proteins, and so on. According to Porod's law,[1,2] the intensity at the tail region of the SAXS curve decreases in proportion to x^{-4} for structures with sharp phase boundaries, where "x" is the vertical distance of the detector from the plane of the primary beam. However, investigations[3–6] on SAXS show distinct deviations from Porod's law, that is, intensity is found to decrease in proportion to x^{-6} rather than x^{-4}. Ruland[7] presented a method for analyzing the deviations from Porod's law in terms of a model containing two phases and having a transition layer of width E in which electron density varies continuously from matter phase to void phase.

Sisal being a natural cellulosic fiber having macromolecular structure with molecular dimension longer than the wavelength of X-ray, SAXS technique was used to evaluate the fine structural characteristics of the air-dried sisal fiber along with the fibers heated and treated with alkali solutions following the procedures of Misra et al.[4,5] SAXS theories have been widely applied in the field of biopolymers by Petoukhov et al.,[8–10] Martel et al.,[11] to synthetic polymers by Patel et al.[12] and to natural polymers by Khan et al.[13] In recent years, SAXS techniques proved to be potential tools in the field of nanostructured materials as evident from the works of Marega et al.,[14] Neppalli et al.,[15] Causin et al.,[16] Gilbert et al.,[17] and many more.

The SAXS intensity patterns of sisal fibers both treated and untreated show deviation from Porod's law, establishing that sisal fiber falls under nonideal two-phase structure characterized by continuous variation of electron density at the phase boundary. Therefore, the mean square electron density gradient $\langle|\nabla\eta|^2\rangle$ is proportional to the third moment $\int x^3\tilde{I}(x)dx$ of the smeared out SAXS intensity distribution in reciprocal space and to the second derivative of the correlation functions at the origin.[18] The correlation functions are the Fourier transformation of the SAXS pattern, which contain all the information regarding the scattering particles. The structural changes due to heat and alkali treatments are interpreted in terms of macromolecular parameters, determined by using SAXS techniques.

SAMPLES

Sisal is a hard vegetable fiber obtained from the leaves of the plant agave sisalana, growing mainly

Correspondence to: Md. N. Khan (mdnkhan1964@gmail.com). .

in tropical countries. The fiber is extracted from the matured leaves by decortication. This fiber is now world's most important leafy fiber comprising of more than half of the total commercial production of all leaf textile fibers. It is not only a hard currency earner but also finds extensive use in navies, fisheries, garments, and so on. The sample investigated was obtained from Sisal Research Station, Bamara, Orissa, India. To acquire pure scattering pattern of sisal fiber due to the principal cellulose component, the fiber was dewaxed following the method of Roy.[19] Further, it also imparts a "hohlraum character," that is, material was packed in layers like the pages of a book.[20] In cellulosic natural fibers, the long axes of the microcrystallites form a constant angle with the fiber axis so that the samples can be taken as a two-phase densely packed highly oriented system.[21] The dewaxed sample heated at temperatures 60, 75, and 90°C for 24 h are named as Sisal-60°C, Sisal-75°C, and Sisal-90°C, respectively. The samples soaked in NaOH solution for 90 h at pH values 11, 12, and 13 and then air dried are referred as Sisal-pH11, Sisal-pH12, and Sisal-pH13, respectively. The air dried untreated sisal fiber is known as Sisal-AD. All the samples were kept in desiccator as cellulosic natural fibers are hygroscopic in nature.

EXPERIMENTAL

The SAXS measurements were taken by a compact Kratky camera, "Anton Paar KG, A-8054, GRAZ, AUSTRIA-EUROPA," using a "Phillips PW-1729 X-ray generator" with entrance slit of 150 μm, counter slit of 375 μm, and a copper target operated at 40 kV and 30 mA. The monochromatization was achieved using a nickel filter of 10 μm thick. The samples were irradiated with $CuK_\alpha(\lambda = 1.54 \times 10^{-10}$ nm) radiation. The body of the compact camera forms a tightly sealed evacuated space, which encases all the construction units except the registration device, which in our case was a proportional counter. The X-ray radiation enters this space through a 0.25 μm-thick beryllium window from the front side and scattered radiation leaves through a similar window at the opposite side. By this construction, the entire radiation path between the two windows runs through vacuum, thus avoiding scattering by air molecules. The distance of the samples from the counter slit was 20 cm and the temperature of the room was maintained at 22.5°C by an air conditioner.

THEORY

The detailed theory and procedures of this SAXS investigation have been described in the previous works of Misra et al.[4,5] on air-dried sisal and cotton, respectively. The straightforward formulae to compute the various macromolecular parameters of heated and alkali-treated sisal fibers are outlined below.

In the evaluation of various macromolecular parameters, the characteristic parameter R is given by

$$R = \frac{3}{2}\left(\frac{2\pi}{\lambda a}\right)^2 \frac{\int_0^\infty x^3 \tilde{I}(x)dx}{\int_0^\infty x\tilde{I}(x)dx} \quad (1)$$

where x represents the position coordinates of the scattered intensity from the center of the primary beam and "a" represents the distance between sample and detector slit. The ratio R is a useful parameter for characterization of macromolecular structures. In ideal two-phase structures, the gradient at the phase boundary is infinity and consequently R goes to infinity. On the other hand, if R is finite, the electron density changes from one phase to other continuously over a transition layer of width E.

The three-dimensional correlation function $C(r)$, which gives the relation between macromolecular structure and SAXS intensity pattern, given by Merring et al.[22] modified by Misra et al.,[4,5] can be written as

$$C(r) = \frac{\int x\tilde{I}(x)J_0(kxr)dx}{\int x\tilde{I}(x)dx} \quad (2)$$

J_0 is the Bessel function of first kind and zero order. The characteristic parameter R as given by Vonk[18] is

$$R_V = -3\left(\frac{d^2C(r)}{dr^2}\right)_{r=0} \quad (3)$$

The value of E, the width of transition layer can be obtained from the three-dimensional correlation function of the sample normalized to unit at the origin in real space. The relation given by Vonk[18] for the width of transition layer is

$$E_V = -\frac{4}{R}\left(\frac{dC(r)}{dr}\right)_{r=E_V} \quad (4)$$

In order to obtain E_v, it is required to calculate the values of $C(r)$ for various values of r in real space.

For a layer structure, Kortleve et al.[23] have shown the use of one-dimensional correlation function $C_1(y)$. The expression for $C_1(y)$ is given according to Mering et al.[22] and modified by Misra et al.,[4,5] can be written as

$$C_1(y) = \frac{\int_0^\infty x\tilde{I}(x)[J_0(z) - zJ_1(z)]dx}{\int_0^\infty x\tilde{I}(x)dx} \quad (5)$$

where $z = \frac{2\pi xy}{a}$ and J_1 is the Bessel function of first-order and first kind. According to Vonk,[18] the position of first subsidiary maximum in one-dimensional correlation function $C_1(y)$ gives the value of the average periodicity transverse to the layers.

According to Vonk,[18] relation between correlation functions $C(r)$ and $C_1(y)$ at origin exists and is given as

$$3\left(\frac{d^2C(r)}{dr^2}\right)_{r=0} = \left(\frac{d^2C_1(y)}{dy^2}\right)_{y=0} \quad (6)$$

Using the following relation given by Vonk[18]

$$\frac{(\Delta\eta)^2}{\langle\eta^2\rangle} = -D\left(\frac{dC_1(y)}{dy}\right)_{y>E_V} \quad (7)$$

the value of $\frac{(\Delta\eta)^2}{\langle\eta^2\rangle}$ can be computed, where $\Delta\eta$ is the electron density difference between the two phases.

According to Vonk[18] for nonideal two-phase structure the relation

$$\varphi_1\varphi_2 = \frac{\langle\eta\rangle^2}{(\Delta\eta)^2} + \frac{E_V}{3D} \quad (8)$$

holds good. Here φ_1 and φ_2 are the volume fractions of the matter and void phases, respectively. For this purpose, the phase boundary is chosen at the middle of the transition layer. Taking the sum of the volume fractions of the two phases to be unity, relations (7) and (8) can be used to get the values of φ_1 and φ_2 as

$$\varphi_1 = \frac{1 + \sqrt{1 - 4\varphi_1\varphi_2}}{2} \quad (9)$$

$$\varphi_2 = \frac{1 - \sqrt{1 - 4\varphi_1\varphi_2}}{2} \quad (10)$$

The distance statistics can be worked out according to Porod[1,2] for the calculation of the transversal lengths. In an irregular two-phase system, if arrows are shot in all possible directions, the average intersection lengths of the arrows in two phases are called transversal lengths and are denoted by ℓ_1 and ℓ_2. According to Mittelbach et al.,[24] the transversal lengths in matter and void phases, respectively, are given by

$$\ell_1 = 4\varphi_1\frac{V}{S} \quad (11)$$

and

$$\ell_2 = 4\varphi_2\frac{V}{S} \quad (12)$$

For a layer structure the specific inner surface S/V is defined as the surface of the phase boundary per unit volume of the dispersed phase and is given by Vonk[18] as

$$\frac{S}{V} = \frac{2}{D} \quad (13)$$

A second method for the estimation of the value of width of transition layer is given by Vonk.[18] The functional relation of $\tilde{I}(x)$ with x at the tail region of SAXS pattern for a nonideal two-phase system is given by

$$x\tilde{I}(x) = \frac{\pi c}{2}(\lambda a)^3 x^{-2} - \frac{\lambda ac\pi^3 E^2}{3} \quad (14)$$

where "c" is a proportionality constant. The value of E_R, the width of transition layer can be calculated from Ruland plot (plot of $x\tilde{I}(x)$ versus x^{-2}) by least square method of fitting straight line at tail region data of SAXS pattern.

Background correction

In every SAXS experiment, a continuous background scattering is always superimposed over the SAXS pattern of the sample. Both Vonk and Ruland methods of estimation of width of transition layer yield results, which are sensitive to errors in the tail region of SAXS pattern. The correlation functions at the origin are also very sensitive to the errors at the tail region of SAXS curve. Therefore, care has been taken to separate SAXS intensities $\tilde{I}(x)$ from the continuous background scattering $\tilde{I}_{bg}(x)$. In the SAXS patterns of all the samples in the domain of our investigation, intensity values at the tail region of the SAXS curve remain constant where X-ray scattering due to samples are very small. So, one is justified in deducting a constant background intensity corresponding to the minimum intensity value in SAXS pattern. These background corrected data at the tail region must be subjected to the following two conditions to show their correctness. The standard deviation σ[25] at the tail region must be below 0.5 and coefficient of line regression γ[4–6] in the same region must approach unity. These background-corrected SAXS intensities have been used in our subsequent analysis.

Calculations

Because of instrumental limitations, SAXS data cannot be collected up to zero angle. Therefore, initial five intensity data of each sample were fitted to Gaussian curve of the form $\tilde{I}(x \to 0) = pe^{-qx^2}$ by least square method. The values of p and q thus found

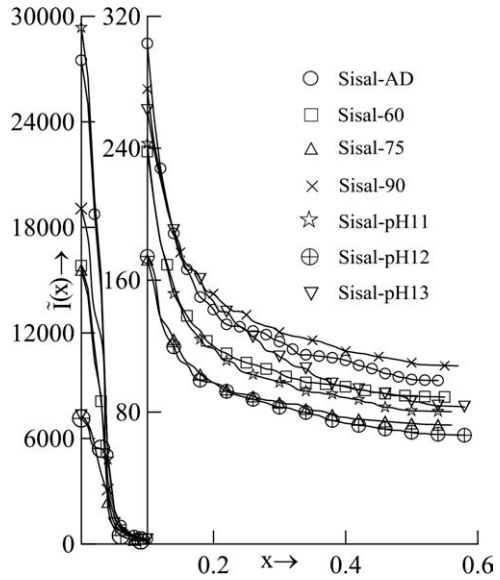

Figure 1 The smeared-out SAXS patterns of sisal fibers.

out and used in the same equation to obtain scattering patterns towards zero angles for all samples under the purview of our study. The complete scattering patterns of all the samples are shown in Figure 1. As shown in the Table I, the standard deviation σ and the coefficient of line of regression γ for each sample have optimum values and prove the error free collection of SAXS data at the tail region of SAXS pattern to which correlation functions at the origin are very sensitive to errors. The negative intercept obtained from the Ruland plot and finite value of R and R_V suggest that all the samples under investigation possess nonideal two-phase structure.

The two integrals in the relation (1) and all other integrals were calculated by numerical methods by applying Simpson's one-third rule. Using the relation (2), $C(r)$ was computed for various values of r for all samples and shown in Figure 2. Then $-[(4/R)(dC(r)/dr)]$ for all samples were computed by numerical differentiation method using five-point central difference formula with a constant interval of 10^{-1} nm and are shown in Figure 3. The points at which a unit slope straight line intersects these curves give the values of width of transition layers E_v by Vonk method. Like other natural cellulosic fibers, sisal possesses a layer structure and hence one-dimensional correlation function $C_1(y)$ was computed for various values of y using relation (5) and shown in Figure 4. The values of D, the average periodicity transverse to the layers for all the samples were obtained from the first subsidiary maximum of this plot. With the help of relation (13), the value of S/V, the specific inner surface was calculated for all the samples. The second differential coefficients of one- and three-dimensional correlation functions at origins, that is, $\left([d^2C_1(y)]/dy^2\right)_{y=0}$ and $\left([d^2C(r)]/dr^2\right)_{r=0}$ of each sample were determined by using five-point forward difference double differentiation formula. The slopes $([dC_1(y)]/dy)_{y\geq E_V}$ calculated by numerical methods were found to be nearly constant for each sample separately. From the relation (7), the values of $(\Delta\eta)^2/\langle\eta^2\rangle$ for each sample were computed and the volume fractions and transversal lengths in both phases were computed with the help of relations (9, 10, 11, 12), respectively. The Ruland plot for all the samples were shown in Figure 5 where straight lines have been fitted by least square technique at the tail region of the SAXS patterns. Making the use of slopes and y-intercepts of each line, the values of width of transition layers E_R were calculated.

RESULTS AND DISCUSSION

The results have been computed using the detailed theories and procedures outlined above. The relevant constants are tabulated in Table I. The macromolecular parameters for heated and alkali (NaOH)-treated samples were shown in Table II along with air dried sisal fiber for comparison. Most of the macromolecular parameters investigated are pictorially represented in Figure 6. This figure depicts the physical meanings of periodicity transverse to layers D, width of transition layer E, transversal length in

TABLE I
The Relevant Constants of Air-Dried and Heat- and Alkali-Treated Samples of Sisal Fibers

Samples→ constants↓	Sisal-AD	Sisal-60°C	Sisal-75°C	Sisal-90°C	Sisal-pH11	Sisal-pH12	Sisal-pH13	Units
p	27512.563	15827.734	15596.594	19064.723	29354.912	7135.598	7304.912	
q	958.77	874.60	1016.86	914.96	1001.86	698.37	665.33	
I_{bg}	99.12	89.11	71.83	108.01	80.27	66.02	108.01	
$\sigma(R)$	0.15	0.04	0.03	0.01	0.02	0.02	0.03	
R	7.26	7.08	7.60	8.82	5.58	12.9	18.90	$\times 10^{-5}$ nm^{-2}
R_v	7.35	7.17	7.71	8.88	5.57	12.99	18.96	$\times 10^{-5}$ nm^{-2}
$\left([d^2C(r)]/dr^2\right)_{r=0}$	−2.45	−2.39	−2.57	−2.96	−1.86	−4.33	−6.32	$\times 10^{-5}$ nm^{-2}
$\left([d^2C_1(y)]/dy^2\right)_{y=0}$	−7.32	−7.08	−7.58	−8.79	−5.72	−12.89	−18.89	$\times 10^{-5}$ nm^{-2}
γ	0.96	0.91	0.92	0.90	0.94	0.97	0.93	

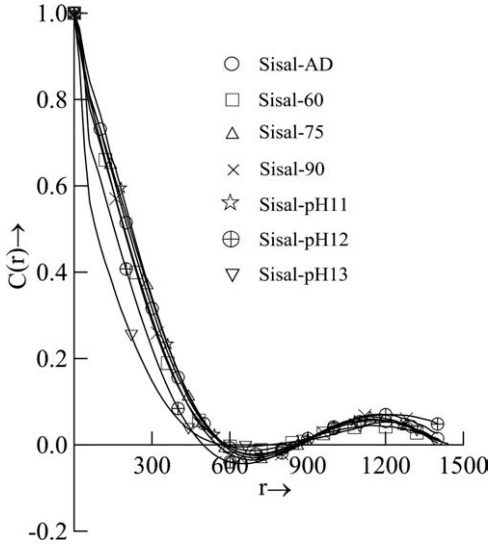

Figure 2 Three-dimensional correlation functions of sisal fibers.

matter phase ℓ_1, transversal length in void phase ℓ_2, volume fraction of matter phase φ_1, and volume fraction of void phase φ_2.

The standard deviation σ[25] of the scattering data at the tail-region for all the investigated samples came out to be much less than the permissible value of 0.5. Besides, the coefficient of line of regression γ[4–6] for all the samples approaches unity in the aforesaid region. The above results show the correctness of collected SAXS data at the tail region at which correlation functions are most sensitive. The value of the characteristic parameter R for each sample is finite, which suggests the nonideal structure of

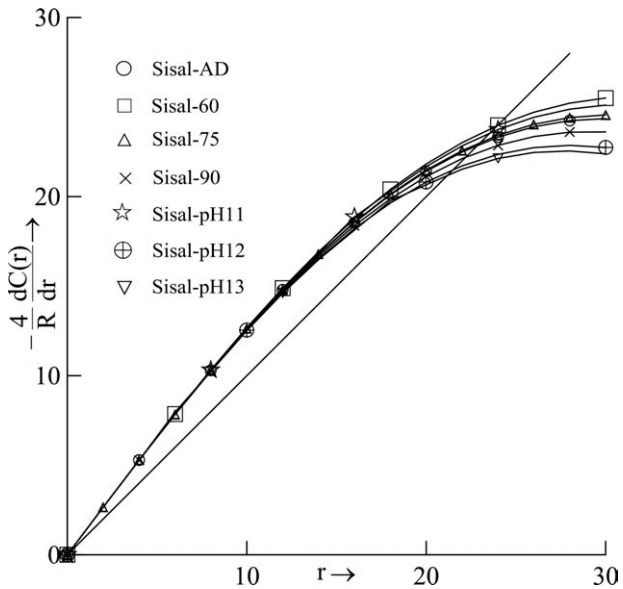

Figure 3 The curves showing the values of $-[(4/R)(dC(r)/dr)]$ against "r" values. The straight line is an equidistant line from both the axes.

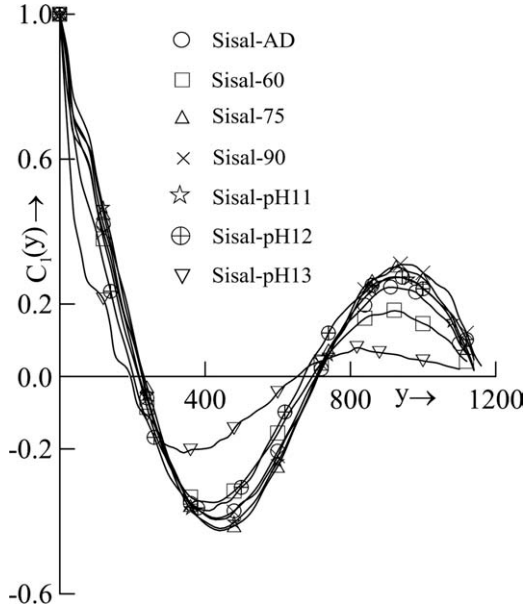

Figure 4 One-dimensional correlation functions of sisal fibers.

all samples.[18] The values of (R, R_v) and (E_v, E_R) evaluated by two different methods are nearly equal. This proves the correctness of our analysis. There is a good agreement in the values of $3\frac{d^2C(r)}{dr^2}\Big|_{r=0}$ and $\frac{d^2C_1(y)}{dy^2}\Big|_{y=0}$ for all the samples under our purview of investigation (Table I). This favors the discussion of Kratky et al.[26] that cellulosic samples are isotropic in nature.

The value of width of transition layer of each sample calculated by two different methods (relations 4, 14) is nearly equal. This indicates the correctness of our approach. Again, there is no significant variation

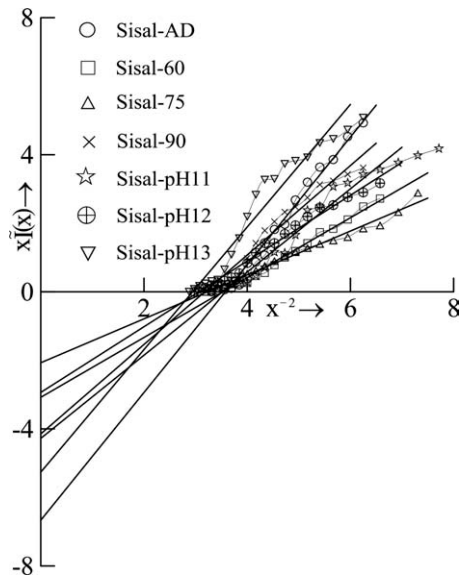

Figure 5 The plot of $x\tilde{I}(x)$ versus x^{-2}.

TABLE II
The Effect of Heat and Alkali on Various Macromolecular Parameters of Sisal Fiber

Samples→ Parameters ↓	Sisal-AD	Sisal-60°C	Sisal-75°C	Sisal-90°C	Sisal-pH11	Sisal-pH12	Sisal-pH13	Units
D	911	921	926	939	919	944	819	$\times 10^{-1}$ nm
S/V	2.19	2.17	2.16	2.13	2.18	2.12	2.44	$\times 10^{-2}$ nm^{-1}
E_v	22.29	23.98	23.03	22.12	23.75	21.30	21.13	$\times 10^{-1}$ nm
E_R	22.65	22.59	21.61	21.42	22.30	21.03	20.48	$\times 10^{-1}$ nm
$2E_v/D$	4.97	5.21	4.97	4.71	5.17	4.51	5.16	%
ϕ_1	86.32	86.79	87.02	88.88	88.15	93.63	92.27	%
φ_2	13.68	13.21	12.98	11.12	11.85	6.37	7.73	%
ℓ_1	1572.75	1598.67	1611.55	1669.14	1620.20	1742.14	1533.63	$\times 10^{-1}$ nm
ℓ_2	249.24	243.33	240.45	208.86	217.80	145.86	104.37	$\times 10^{-1}$ nm

in the values of width of transition layer of all the samples. This means that heat and alkali have no remarkable effects on the corrugation of phase boundary.

The values of D, the periodicity transverse to layers for heat-treated samples increases with the rise in temperature. This shows the swelling behavior of particles under action of heat. In alkali-treated samples the periodicity transverse to layers increases with increase in the pH value of alkali solution showing the swelling of particles. However, at pH = 13, the same parameter decreases. The reason for this may be due to the rupture of particles producing particles of different dimension.

There is no remarkable change in the value of $\frac{2E_V}{D}$, the volume fraction of transition layer for all the samples. It is a measure of the degree of corrugation of the phase boundary. This indicates that heat and alkali have no significant effects on the degree of corrugation of the phase boundary.

The specific inner surface $\frac{S}{V}$ for heat-treated samples decreases with the rise in temperature. This means that particles swell under action of heat. In alkali-treated samples, the specific inner surface decreases with increase in the pH value of alkali solution. This shows the swelling nature of particles with rise in concentration of alkali solution. However, at pH = 13, the same parameter increases. This result indicates that cellulosic particles break at pH value of 13 of alkali solution.

The increase in the value of φ_1, the volume fraction of matter phase with temperature suggests the swelling property of matter phase. In addition, for the same reason, the same parameter increases with the increase in the pH value of the alkali solution. As at pH = 13, the particles rupture producing new particles, having different dimension from the original ones, the volume fraction of matter phase decreases. The volume fraction of void phase φ_2, changes in opposite manner as that discussed for φ_1 values. The transversal lengths ℓ_1 and ℓ_2 in the matter and void phases, respectively, changes in accordance with the values of φ_1 and φ_2, respectively, along with the D values except for the alkali treated fiber at pH = 13. The transversal length in void phase ℓ_2 has the same meaning as that of average size of microvoid and is found to decrease with increase in temperature. This conclusion is in consistent with the above discussion.

Similar trend in the variation of macromolecular parameters are also observed when air-dried sisal fiber is taken into account, justifying our approaches and analysis. Based on the detailed analysis described above, a statistical lamellar model of sisal fiber[5] has been represented by Figure 6 depicting almost all the macromolecular parameters.

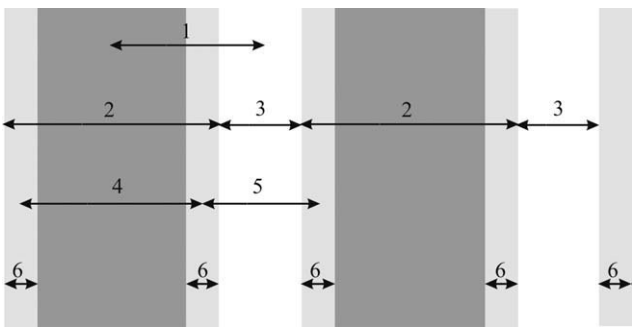

Figure 6 Statistical lamellar model of sisal fiber: (1) Periodicity transverse to layers, (2) Matter phase, (3) Void phase, (4) Transversal length in matter phase, (5) Transversal length in void phase, (6) Width of transition layer.

CONCLUSIONS

From the above calculations and results, it has been inferred that air-dried, heated, and alkali-treated sisal fibers are nonideal two-phase systems. The matter phase in sisal fiber swells with increasing temperatures and also when treated with NaOH solutions of increasing concentrations. Heat and NaOH solutions do not affect the corrugation of phase boundaries between matter and void phases of sisal fiber even though phases breaks at pH = 13.

References

1. Porod, G. Kolloid Z 1951, 124, 83.
2. Porod, G. Kolloid Z 1952, 125, 51.
3. Tavernier, S. M. F.; Vonk, C. G.; Gijbels, R. J Colloid Interface Sci 1981, 81, 341.
4. Misra, T.; Bisoyi, D. K.; Patel, T.; Patra, K. C.; Patel, A. Polym J 1988, 20, 739.
5. Misra, T.; Khan, Md. N.; Patel, T.; Bhatt, N. V. J Appl Phys 1991, 24, 331.
6. Misra, T.; Bisoyi, D. K.; Khan, Md. N.; Patel, T. J Appl Crystallogr 1991, 24, 712.
7. Ruland, W. J Appl Crystallogr 1971, 4, 70.
8. Petoukhov, M. V.; Vicente, J. B.; Crowley, P. B.; Carrondo, M. A.; Teixeira, M.; Svergun, D. I. Structure 2008, 16, 1428.
9. Petoukhov, M. V.; Svergun, D. I. Curr Opin Struct Biol 2007, 17, 562.
10. Petoukhov, M. V.; Svergun, D. I. Euro Biophys J 2006, 35, 567.
11. Martel, A.; Burghammer, M.; Davies, R. J.; Di Cola, E.; Vendrely, C.; Riekel, C. J Am Chem Soc 2008, 130, 17070.
12. Patel, T.; Ball, S. Polym J 2001, 33, 121.
13. Khan, Md. N.; Bisoyi, D. K.; Shuckla, J.; Sahoo, R. Fibers Polym 2011, 12, 765.
14. Marega, C.; Causin, V.; Marigo, A. J Appl Polym Sci 2008, 109, 32.
15. Neppalli, R.; Causin, V.; Marega, C.; Saini, R.; Mba, M.; Marigo, A. Polym Eng Sci 2011, 52, 2489.
16. Causin, V.; Marega, C.; Marigo, A.; Ferrara, G.; Ferraro, A.; Selleri, R. J Nanosci Nanotechnol 2008, 8, 1823.
17. Gilbert, B.; Reyn, K. O.; Kristen, A. C.; Christopher, S. K. J Colloid Interface Sci 2009, 339, 285.
18. Vonk, C. G. J Appl Crystallogr 1973, 6, 81.
19. Roy, S. C. Text Res J 1960, 30, 451.
20. Kahovec, L.; Porod, G.; Ruck, H. Kolloid Z Z Polym 1953, 133, 16.
21. Kratky, O. In Small Angle X-ray Scattering; Glatter, O., Kratky, O., Eds.; Academic Press: London, 1982; p 361.
22. Mering, J.; Tchoubar, D. J Appl Crystallogr 1968, 1, 153.
23. Kortleve, G.; Vonk, C. G. Kolloid Z Z Polym 1968, 225, 124.
24. Mittelbach, P.; Porod, G. Kolloid Z Z Polym 1965, 202, 40.
25. Vonk, C. G. J Appl Crystallogr 1971, 4, 340.
26. Kratky, O.; Stabinger, H. Colloid Polym Sci 1984, 262, 345.